THE JOURNAL OF PHYSICAL CHEMISTRY B
A JOURNAL OF THE AMERICAN CHEMICAL SOCIETY

pubs.acs.org/JPCB

Article

Excited-State Dynamics of a Substituted Fluorene Derivative. The Central Role of Hydrogen Bonding Interactions with the Solvent

Briana A. Capistran, Stephen H. Yuwono, Mehdi Moemeni, Soham Maity, Aria Vahdani, Babak Borhan, James E. Jackson, Piotr Piecuch, Marcos Dantus, and G. J. Blanchard*

Cite This: https://doi.org/10.1021/acs.jpcb.1c06474

Read Online

ACCESS | Metrics & More | Article Recommendations

ABSTRACT: Substituted fluorene structures have demonstrated unusual photochemical properties. Previous reports on the substituted fluorene Schiff base **FR0**-SB demonstrated super photobase behavior with a ΔpK_b of ~14 upon photoexcitation. In an effort to understand the basis for this unusual behavior, we have examined the electronic structure and relaxation dynamics of the structural precursor of **FR0**-SB, the aldehyde **FR0**, in protic and aprotic solvents using time-resolved fluorescence spectroscopy and quantum chemical calculations. The calculations show three excited singlet states in relatively close energetic proximity. The spectroscopic data are consistent with relaxation dynamics from these electronic states that depend on the presence and concentration of solvent hydroxyl functionality. These results underscore the central role of solvent hydrogen bonding to the **FR0** aldehyde oxygen in mediating the relaxation dynamics within this molecule.

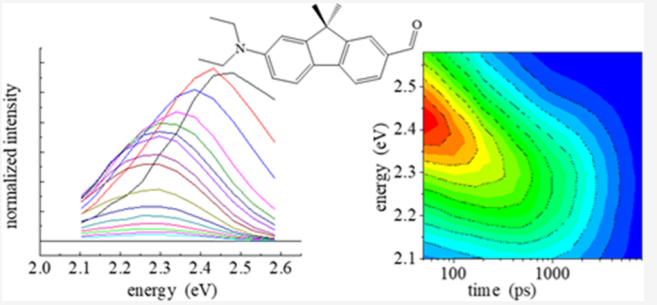

INTRODUCTION

Chemical reactions are typically performed in the liquid phase or at the interface between phases with reactants in their ground states. Under such conditions there is little opportunity for temporal or spatial control of the reaction, although photochemical activation of one reactant is often best suited to achieve this. Nonetheless, the use of the latter strategy has historically been limited. Therefore, by gaining broader utility in photochemical reactions one affords new opportunities for temporal and spatial control of reaction chemistry, properties that are central to the emerging fields of precision chemistry and high-speed chemical sensing.

Most chemical reactions are either acid−base (proton transfer) or redox (electron transfer) reactions. The ability to alter the acidity or basicity of certain compounds through photoexcitation has been explored extensively for photoacids, which are photoactivated proton donors,[1,2] but the development of their photobase counterparts, which are able to abstract available protons from their local environment upon photoexcitation, has been much more limited.[3,4] Recently, we have focused on the design and characterization of the super photobase **FR0**-SB[5−8] that is capable of exhibiting a remarkable increase in K_b of 14 orders of magnitude (or $\Delta pK_b \sim 14$) upon photoexcitation. The behavior of **FR0**-SB (Figure 1a) in protic and aprotic media has been reported recently,[5−7] providing fundamental insights into the proton abstraction reaction that occurs in protic solvents. Among the issues that require further investigation is the chemical structural basis for such a large change in the basicity of the imine nitrogen upon photoexcitation. In an effort to understand more completely the structural properties that lead to super photobase behavior, we have examined the excited-state properties of the aldehyde precursor of **FR0**-SB, namely, **FR0** (Figure 1b).

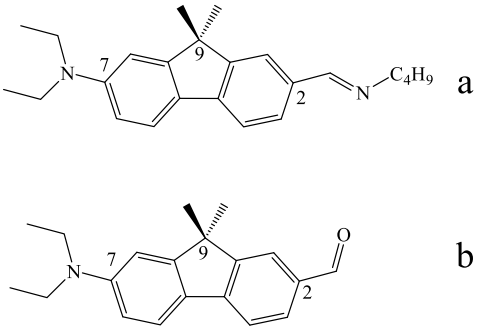

Figure 1. Molecular structures of (a) **FR0**-SB Schiff base and (b) **FR0** precursor.

Received: July 20, 2021
Revised: October 11, 2021

A comprehensive understanding of the reactivity and excited-state population relaxation dynamics of such precursor molecules is a key step toward the rational design of super photobases with controlled properties for specific applications. In this work, we report on the reactivity and excited-state relaxation dynamics of the **FR0** precursor molecule in protic and aprotic solvent media using steady-state and time-resolved spectroscopy in conjunction with quantum chemical computational results.

The spectroscopic properties of the super photobase **FR0**-SB make the study of its photoreactivity relatively straightforward. Emission bands for unprotonated and protonated forms of the photoexcited Schiff base **FR0**-SB* are well resolved, and the time evolution of those band intensities provides direct insights into solvent proton abstraction by **FR0**-SB*. The data reported here for **FR0** also exhibit spectral dynamics, although the resolution of individual bands is not as facile. The emission spectrum of **FR0** exhibits time-dependent changes in the band shape and position in protic solvents, suggesting a significant role of the **FR0** chromophore structure in the unusual photobase behavior of the corresponding Schiff base. We report on the presence of the overlapped electronic singlet state manifolds within the **FR0** emission band and population exchange between those singlet states in protic solvents. The excited-state relaxation dynamics of **FR0** depend on the identity of the (protic) solvent. Spectral reconstruction from the time-resolved emission data reveals the details of band evolution and demonstrates that the relaxation dynamics of the **FR0** precursor molecule are mediated by hydrogen-bonding interactions between **FR0** and the surrounding solvent medium.

EXPERIMENTAL METHODS

Materials. *n*-Propanol (99.7%, anhydrous), *n*-pentanol (≥99%, ACS grade), and dimethyl sulfoxide (DMSO, ≥99.9%, anhydrous) were all purchased from Sigma-Aldrich and used as received. *n*-Pentanol, which was not available in an anhydrous form, was stored over molecular sieves (type 3A).

Synthesis of FR0. The synthesis of **FR0** followed the procedure reported previously[8,9] and is described briefly here. The synthesis commenced with fluorene, which was converted to 2-bromofluorene by treating with *N*-bromosuccinimide in propylene carbonate at room temperature. Dimethylation of the C9 position was accomplished with the treatment of the brominated fluorene with excess iodomethane in the presence of NaOH. Fuming nitric acid was used for the nitration of the nonbrominated aryl ring to yield 2-bromo-9,9-dimethyl-7-nitro-9*H*-fluorene. Subsequent reduction of the nitro group with iron powder suspended in aqueous ammonium chloride solution provided the corresponding amine. The resulting product was heated with ethyl iodide and potassium carbonate generating the diethyl amino substituent. Metal/halogen exchange promoted by the addition of *n*-BuLi, followed by the addition of dimethylformamide led to the formation of **FR0**. Purification of the crude on a silica-gel column (hexane/ethyl acetate eluant) provided the title compound as a yellow solid. ^{1}H NMR (500 MHz, $CDCl_3$): δ (ppm) = 9.98 (d, J = 0.8 7.90−7.85 (m, 1H)), 7.78 (dt, J_1 = 7.8 Hz, J_2 = 1.1 Hz, 1H), 7.68−7.59 (m, 2H), 6.73−6.66 (m, 2H), 3.46 (q, J = 7.1 Hz, 4H), 1.50 (s, 6H), 1.30−1.20 (m, 7H). ^{13}C NMR (125 MHz, $CDCl_3$): δ (ppm) = 192.05, 157.33, 153.19, 148.99, 146.90, 133.41, 131.27, 125.20, 122.47, 122.35, 118.12, 110.87, 105.06, 46.62, 44.71, 27.24, 12.59.

The compound was stored in ethanol (1 mM). To prepare samples of **FR0** in each solvent, aliquots of **FR0** were brought to dryness using nitrogen and reconstituted with the solvent system to be studied at a concentration appropriate for the measurement, typically *ca.* 5×10^{-6} M.

Steady-State Emission Spectroscopy. Emission spectra for **FR0** in each of the solvents were collected using a Hitachi F-4500 fluorescence spectrometer and Spex Fluorolog 3 emission spectrometer. Quartz cuvettes (1 cm) were used for all the measurements and spectra acquired using an excitation wavelength of 440 nm, with an excitation and emission spectral resolution of 1 nm.

Time-Resolved Fluorescence Spectroscopy. Time-resolved fluorescence measurements were collected using a time-correlated single photon counting (TCSPC) instrument that has been described in detail elsewhere,[10,11] and we provide only a brief summary here. The light source is a continuous-wave passively mode-locked Nd:YVO_4 laser (Spectra Physics Vanguard) that produces 13 ps pulses at 1064 nm (80 MHz repetition rate). The output of this laser was at the second harmonic (532 nm) and the third harmonic (355 nm), with 2.5 W of average power at both wavelengths, with the same pulse duration. For the experiments reported here, the cavity-dumped dye laser (Coherent 702-2) was excited by the third harmonic output of the pump laser. The dye used was Stilbene 420 (Exciton) and the dye laser output at 440 nm was 5 ps full-width at half-maximum (fwhm) pulses at a repetition rate of 4 MHz. The pulses from the dye laser were divided with approximately half going to a reference channel diode (Becker & Hickl PHD-400-N) and the remaining light going to the sample. The vertically polarized excitation light was focused on the sample cuvette and a reflecting microscope objective (40×, Ealing) was used to collect emission. The collected emission was passed through a polarization-selective beam splitter and sent to two identical detection channels. Each detection channel had a subtractive double monochromator (Spectral Products CM-112) and a microchannel plate photomultiplier tube (PMT) detector (Hamamatsu R3809U-50). Signals from each detector were sent to TCSPC detection electronics (Becker & Hickl SPC-132). A typical instrument response function for this system is *ca.* 35 ps fwhm. The TCSPC acquisition electronics, PMT bias, and monochromator wavelengths were controlled using a computer program written in-house using LabVIEW (National Instruments) software. For these experiments, time-resolved fluorescence data were acquired from 470 to 620 nm, in 10 nm increments. All raw time-domain data were exported to Microsoft Excel (Microsoft Office 365, Microsoft Corporation, Redmond, WA). Data analysis, including the extraction of fluorescence lifetime decay constants and band fitting, was performed using Microcal Origin (OriginPro 9.0, OriginLab Corporation, Northampton, MA).

COMPUTATIONAL DETAILS

The quantum chemistry calculations performed in this work were based on the computational protocol that has been described in detail in our earlier work.[5] We started by optimizing the geometry of the isolated **FR0** chromophore in its ground electronic state S_0 using the Kohn−Sham[12] formulation of density functional theory,[13] where we employed the CAM-B3LYP[14] functional and the 6-31+G* basis set.[15−17] Subsequently, we used the equation-of-motion (EOM) extension[18] of the coupled-cluster (CC) theory[19] to the

https://doi.org/10.1021/acs.jpcb.1c06474
J. Phys. Chem. B XXXX, XXX, XXX−XXX

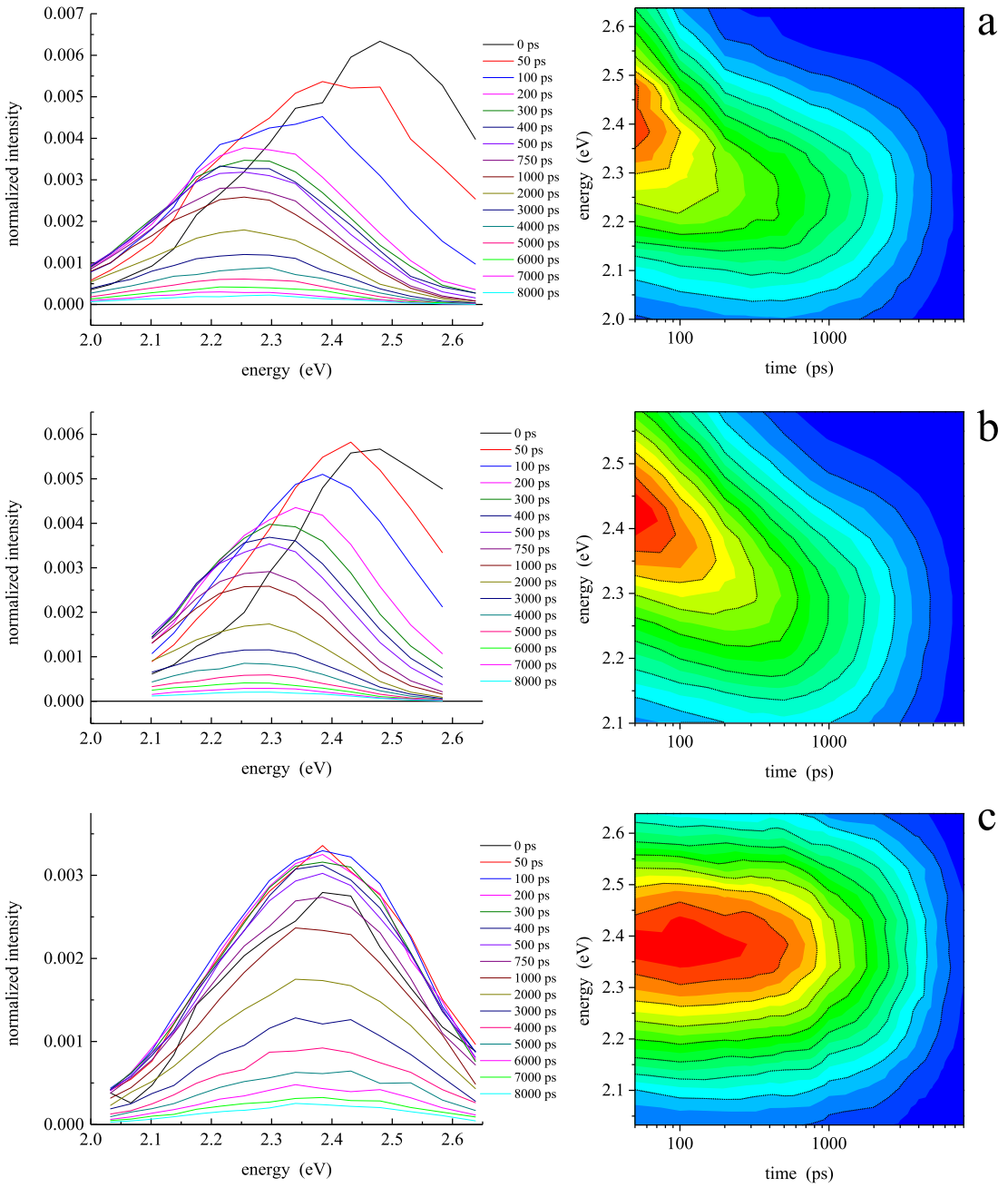

Figure 2. Time-resolved emission spectra of **FR0** in (a) *n*-propanol, (b) *n*-pentanol, and (c) DMSO extracted from experimental fluorescence lifetime data. For the spectra in the left panels, the time corresponding to each spectrum are provided in the legends. The right panels are contour plots of the time-resolved spectra.

excited electronic states to determine the vertical excitation energies characterizing the transitions from the ground state (S_0) to the four lowest excited singlet states (S_n, n = 1−4) of the **FR0** molecule using the composite formula

$$\omega_n^{(\mathrm{EOMCC})} = \omega_n^{(\mathrm{EOMCCSD/6\text{-}31+G^*})} + [\omega_n^{(\delta\text{-CR-EOMCC(2,3)/6-31G})} - \omega_n^{(\mathrm{EOMCCSD/6\text{-}31G})}] \quad (1)$$

The first term on the right-hand side of eq 1 denotes the vertical excitation energy obtained using the EOM extension of the CC method with singles and doubles (CCSD),[20] designated as EOMCCSD,[18] in conjunction with the 6-31+G* basis set. The next two terms on the right-hand side of eq 1 correct the EOMCCSD/6-31+G* results for the higher order many-electron correlation effects due to triple excitations, represented in this work by the δ-CR-EOMCC-(2,3) approach,[21−23] computed at the smaller 6-31G basis set.[15] We also used the CCSD/6-31+G* and EOMCCSD/6-31+G* one-electron reduced density matrices to determine the Mulliken atomic charges, permanent dipole moments, and total electron densities characterizing the ground and excited states, as well as the transition dipole moments (TDMs) and oscillator strengths (OSs) associated with the vertical $S_m \rightarrow S_n$ excitations involving the lowest four excited singlet states of **FR0**.

https://doi.org/10.1021/acs.jpcb.1c06474
J. Phys. Chem. B XXXX, XXX, XXX−XXX

All electronic structure calculations for the **FR0** molecule reported in this work were performed using GAMESS.[24,25] The relevant CCSD, EOMCCSD, and δ-CR-EOMCC(2,3) computations using the restricted Hartree−Fock (RHF) determinant as a reference and the corresponding left-eigenstate CCSD and EOMCCSD calculations, required to obtain the triples corrections of δ-CR-EOMCC(2,3) and the one-electron properties of interest, were performed using the CC/EOMCC routines developed by the Piecuch group,[22,26−28] which form part of the GAMESS code. In all the post-RHF calculations, the core orbitals corresponding to the 1s shells of the C, N, and O atoms were kept frozen. In the calculations employing the 6-31+G* basis set, we used the spherical d-type polarization functions. We utilized VMD software[29] to visualize the **FR0** species.

RESULTS AND DISCUSSION

As mentioned in the Introduction section, the super photobase **FR0**-SB exhibits an anomalously large change in its excited-state pK_b[5,7] and among the issues that remain to be resolved is the role that the fluorene derivative chromophore structure plays in producing this behavior. In this work, we investigate the precursor to **FR0**-SB, the aldehyde **FR0** (Figure 1b), which exhibits unusual fluorescence relaxation dynamics in protic solvents. We present the time-resolved spectra for **FR0** in *n*-propanol (Figure 2a), *n*-pentanol (Figure 2b), and DMSO (Figure 2c). These spectra were extracted from the time-domain experimental data with the integrated emission intensity normalized to the steady-state fluorescence spectrum.

For the time-resolved spectral evolution seen with **FR0**-SB, there were well-resolved emission bands corresponding to unprotonated and protonated species,[5−7] but for **FR0** there is no corresponding imine and, consequently, no analogous spectrally resolved features. It is thus important to consider first whether the data shown in Figure 2a,b represent spectral shifts of a single electronic state in time or the evolution of populations in multiple spectrally overlapped bands. There are several factors that point to the latter explanation being correct.

There is a substantial literature related to spectral evolution and its relationship to solvation dynamics.[30−34] One of the few probe molecules that exhibit this effect is Coumarin 153, which has been studied extensively and found to exhibit a time-resolved fluorescence Stokes shift[31−37] that is mediated by solvent relaxation.[30,38] The data for the time-resolved Stokes shift seen for Coumarin 153 resemble, at least qualitatively, the results shown in Figure 2a,b. The observed spectral relaxation for Coumarin 153 correlates with the solvent Debye relaxation time at a scale of *ca.* 50−100 ps, which is somewhat shorter than that of the spectral shift we observe but not necessarily at odds with the relaxation times in normal alcohols.[39] More importantly, the solvent relaxation model used in the interpretation of C153 dynamics presumes that the spectral dynamics are mediated by relaxation along a featureless reaction coordinate, with the time constant for the relaxation being determined by the solvent surrounding the dipolar excited state accommodating the change in the dipole moment orientation and magnitude resulting from excitation.

If other intramolecular processes such as IVR or relaxation between multiple conformers or electronic state manifolds can be shown to contribute, then the spectral relaxation process cannot be assigned to solvent relaxation alone.[37,40−49] Indeed, the interpretation of these data is not a matter of either solvent relaxation or intramolecular relaxation determining the observed spectral dynamics. It is fully expected that both intermolecular and intramolecular relaxation contribute to the observed spectral behavior and, thus, the issue is which of these contributions influences the **FR0** spectral response most prominently. The intermolecular component is reflected in the solvent-dependent dynamics we report, while the intramolecular component is supported by quantum chemical computations and emission wavelength-dependent rotational diffusion data (*vide infra*). The wavelength dependence of the rotational diffusion data is a consequence of different electronic states interacting with the solvent environment according to their different electron density distributions. There are several pieces of information that we consider below, both experimental and computational, that point to the spectral dynamics we report here being understood in the context of intramolecular relaxation dynamics that are mediated by specific intermolecular interactions. In addition to the analysis provided in the following sections, we have taken the time-resolved emission data at several different wavelengths across the **FR0** emission band and have extracted the rotational diffusion time constants from different emission wavelengths. The reorientation time of **FR0** in alcohols exhibits a measurable wavelength dependence. We will return to a more thorough discussion of this point below, but wavelength-dependent reorientation times require the existence of multiple excited electronic states, each with a finite radiative lifetime. We assert that the data result from relaxation from multiple electronic states rather than temporal evolution along a solvent-mediated relaxation coordinate for a single electronic state.

Computational chemistry has demonstrated its importance in understanding molecular-scale phenomena and spectroscopic dynamics of the super photobase **FR0**-SB.[5−7] We have applied the protocol described in the Computational Details section to investigate the electronic structures of the ground state S_0 and four lowest singlet excited states S_n, n = 1−4, of **FR0**. The results of these calculations reveal several interesting features that help us understand the complex spectral dynamics shown in Figure 2. The $S_0 \rightarrow S_n$ vertical excitation energies and permanent dipole moments of the ground and four lowest excited singlet states of **FR0** are reported in Table 1, while the

Table 1. $S_0 \rightarrow S_n$ Vertical Excitation Energies $\omega_n^{(EOMCC)}$ and the Permanent Dipole Moments μ_n Characterizing the Lowest Four Excited Singlet States of FR0 in the Gas Phase[a]

state	$\omega_n^{(EOMCC)}$ (eV)	μ_n (D)
S_1	3.56	15.2
S_2	3.81	2.5
S_3	3.95	10.0
S_4	4.27	7.8

[a]The dipole moment of **FR0** in the ground S_0 state is 6.2 D.

TDMs and OSs characterizing the $S_m \rightarrow S_n$ vertical excitations involving all the calculated states are reported in Table 2. The Mulliken charges are shown for the ground state S_0 (Figure 3a) and excited states S_1 (Figure 3b), S_2 (Figure 3c), and S_3 (Figure 3d), and the comparison of the magnitude and direction of the permanent dipole moments in each state, along with the electron density differences characterizing the $S_0 \rightarrow S_n$ (n = 1−3) vertical excitations, are shown in Figure 4. There are several interesting observations that stem from our calcu-

https://doi.org/10.1021/acs.jpcb.1c06474
J. Phys. Chem. B XXXX, XXX, XXX−XXX

Table 2. TDMs and OSs Characterizing the Vertical Electronic Excitations Involving the Ground and Four Lowest Excited Singlet States of FR0 in the Gas Phase[a]

	initial state							
	S_0		S_1		S_2		S_3	
target state	TDM (D)	OS	TDM (D)	OS	TDM (D)	OS	TDM (D)	OS
S_1	7.5	0.84						
S_2	0.2	0.00	0.2	0.00				
S_3	2.9	0.14	3.4	0.02	0.1	0.00		
S_4	0.5	0.00	0.2	0.00	0.0	0.00	0.8	0.00

[a]Only $S_m \rightarrow S_n$ transitions with $m < n$ are given in the table.

lations. The first one is that, as shown in Table 1, the three lowest excited electronic singlet states are in relatively close energetic proximity, which suggests a facile population relaxation from S_3 to S_2 or S_1 and from S_2 to S_1. The second important result of our calculations is that the S_0, S_1, and S_3 states exhibit relatively similar electron densities for the aldehyde moiety, with the carbonyl oxygen carrying a Mulliken charge of *ca.* −0.4, and, not surprisingly, the dipole moments are oriented along similar axes (see Figures 3 and 4). The S_2 state, however, exhibits a significantly different electron density distribution for the aldehyde group, with the carbonyl oxygen having a Mulliken charge of *ca.* −0.1 and the aldehyde carbon being substantially more negative (*cf.* Figure 3c). These differences in Mulliken charges are reflected in the small permanent dipole moment in S_2 relative to those characterizing the remaining four electronic states considered in our calculations (see Table 1 and Figure 4). These findings are consistent with our experimental data, as discussed below.

The existence of several excited electronic states in close energetic proximity combined with the unusual spectral dynamics in alcohols suggests that these experimental results are accounted for by the population relaxation between the excited electronic states and radiative relaxation from each state, rather than the temporal evolution of a single band. We propose a kinetic model that is consistent with the observed spectroscopic behavior (Figure 5), as defined below:

$$\frac{dS_3}{dt} = -(k_{30} + k_{31} + k_{32})S_3,$$

$$\frac{dS_2}{dt} = k_{32}S_3 - (k_{20} + k_{21})S_2, \text{ and}$$

$$\frac{dS_1}{dt} = k_{31}S_3 + k_{21}S_2 - k_{10}S_1 \quad (2)$$

In this model, the transitions associated with k_{30}, k_{20}, and k_{10} are all considered to be radiative, while the relaxation phenomena described by k_{32}, k_{31}, and k_{21} are non-radiative. We also consider the excitation to be instantaneous. The temporal evolution of the populations of each state is given by

$$S_3(t) = S_3(0)\exp(-(k_{30} + k_{31} + k_{32})t),$$

$$S_2(t) = \left(S_2(0) + \int_0^t k_{32}\exp((k_{20} + k_{21})x)\cdot S_3(x)dx\right) \exp(-(k_{20} + k_{21})t), \text{ and}$$

$$S_1(t) = \left(S_1(0) + \int_0^t \exp(k_{10}x)\cdot(k_{21}S_2(x) + k_{31}S_3(x))dx\right) \exp(-k_{10}t) \quad (3)$$

With the time-resolved intensities of the three bands determined, it is possible to estimate the rate constants for the model shown in Figure 5 and eq 2. Comparing the kinetic model described above to the experimental data is not as straightforward as fitting individual time-resolved fluorescence intensity decays at specific wavelengths. As noted above, the emission spectrum of **FR0** is broad and relatively featureless, and the presence of multiple radiative decays will be complicated by the spectral overlap of unresolved bands. We have fitted the steady-state emission spectra of **FR0** in the solvents used in this work to three Gaussian bands (Figure 6). Using these fitted band energies, we have taken time slices of the normalized time-domain data and have fitted those time-resolved spectra to determine the band intensities of each of the fitted bands as a function of time. In that manner, we extract the time-evolution of each of the three spectral features. Based on the transition energies, we assign the highest, intermediate, and lowest energy bands to be the $S_3 \rightarrow S_0$, $S_2 \rightarrow S_0$, and $S_1 \rightarrow S_0$ emissions, respectively. While not without precedent, it is noteworthy that $S_2 \rightarrow S_0$ emission appears prominently,[50,51] even though the calculated TDM and OS characterizing the $S_0 \rightarrow S_2$ vertical excitation reported in Table 2 are very low. We have given considerable thought to this apparent incongruity. One possible explanation is vibronic intensity borrowing between the closely spaced electronic states,[52−54] which is a well-established phenomenon, known to depend sensitively on the details of solvent−solute interactions that mediate coupling between the electronic state manifolds. Although the details of solvent−solute interactions are beyond the scope of our quantum chemical computations, such intermolecular interactions may play a determining role in defining the functional form of the experimental data. Based on the computational results shown in Tables 1 and 2, the S_2 state is in close proximity to S_1 and S_3, with the energy differences being $\Delta E(S_2 - S_1) = 2017$ cm^{-1} and $\Delta E(S_3 - S_2) = 1129$ cm^{-1}, and the OSs for the relevant $S_0 \rightarrow S_1$ and $S_0 \rightarrow S_3$ transitions of 0.84 and 0.14, respectively, are significant, thereby producing a condition where intensity borrowing is likely. Furthermore, because of the anti-Hermitian nature of the absorption and emission vibronic coupling terms,[53,55] the OS for the emission transitions can be significantly different than those for the absorption transitions and dependent on the details of the solvent mediation of the vibronic transitions.

In addition to the limitations associated with the spectral overlap and modest signal-to-noise ratio, extracting the rate constants from the time-resolved spectral data is inherently underdetermined because we are trying to evaluate six rate constants using the decay profiles of the three bands. For this reason, we apply the following constraints to obtain physically realistic estimates of our rate constants. The first constraint is

https://doi.org/10.1021/acs.jpcb.1c06474
J. Phys. Chem. B XXXX, XXX, XXX−XXX

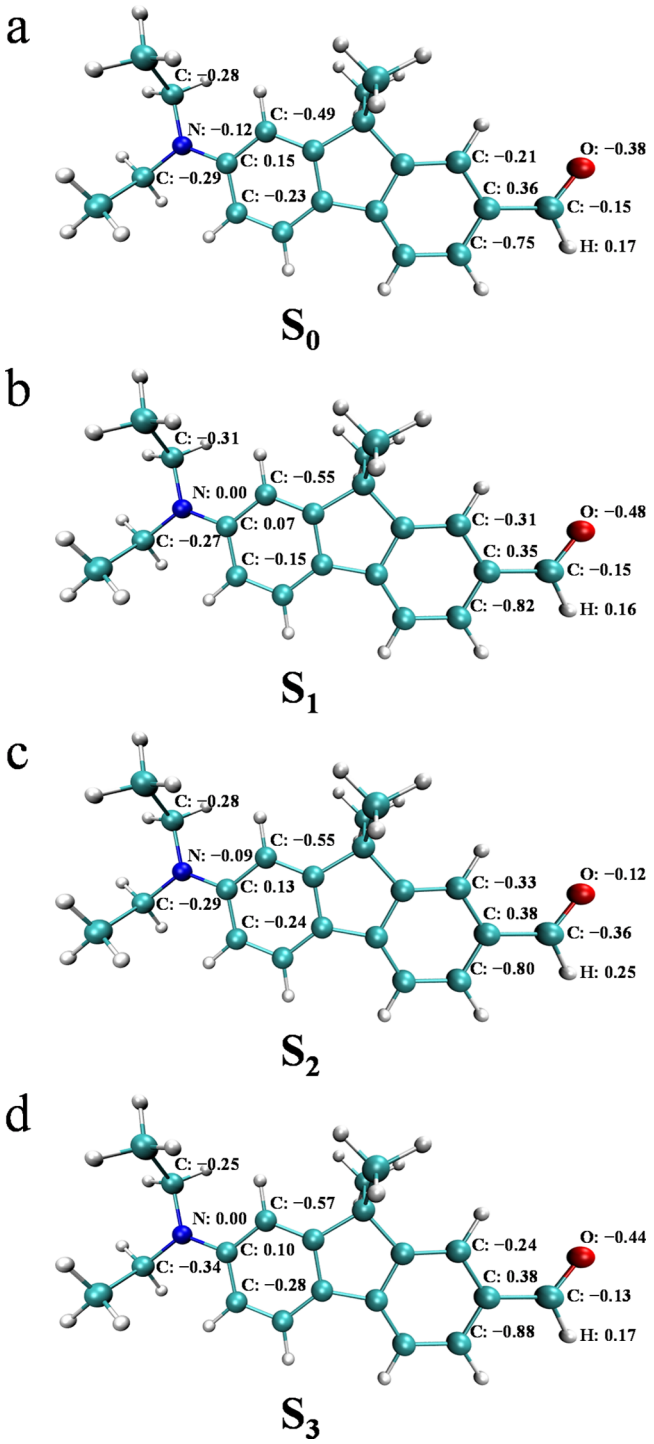

Figure 3. Structure of the isolated **FR0** chromophore in its ground electronic S_0 state and the computed Mulliken charges for the selected atoms in the (a) S_0, (b) S_1, (c) S_2, and (d) S_3 states of **FR0**.

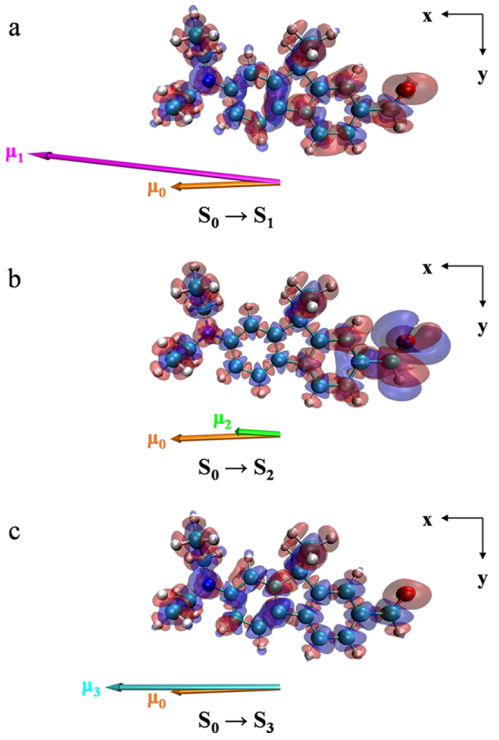

Figure 4. Structure of the isolated **FR0** molecule in its ground electronic S_0 state and the electronic density difference maps associated with the vertical transitions from S_0 to the (a) S_1, (b) S_2, and (c) S_3 states of **FR0**. The red/blue color indicates an increase/decrease in the electron density upon the $S_0 \rightarrow S_n$ (n = 1−3) excitation. The dipole moment vectors characterizing the S_0 (orange), S_1 (magenta), S_2 (green), and S_3 (cyan) states of **FR0** are shown as well.

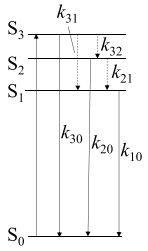

Figure 5. Proposed kinetic model for the excitation and relaxation of **FR0** to the lowest three excited singlet states, in which k_{mn} denotes the rate constant associated with each $S_m \rightarrow S_n$ transition. Dashed arrows represent radiative decays and solid arrows represent non-radiative decays.

that all rate constants must be greater than or equal to zero. The second constraint is that the lifetime of the first excited singlet state, S_1, is on the order of several nanoseconds (*i.e.*, $k_{10} \leq 10^9$). With these basic constraints, we have used a Monte Carlo fitting routine (coded in-house) to estimate the rate constants for the temporal evolution of the fitted emission bands (Table 3). The uncertainties ($\pm 1\sigma$) are based on at least 10 individual determinations for each rate constant. The fits of eq 2 to the experimental data using the rate constants in Table 3 are shown in Figure 7. The agreement between the fitted and experimental data is not exact for reasons of the unaccounted for spectral overlap and the limited signal-to-noise ratio of the measured data. We note that the spectral dynamics we have discussed to this point are seen in protic solvents but not in aprotic solvents, such as DMSO. Based on this information, we assert that the spectral dynamics we observe are associated with hydrogen bonding between the solvent molecules and the **FR0** chromophore.

While the ability of the solvent to form hydrogen bonds with **FR0** is related to the observed spectral dynamics, it is important to consider whether solvent viscosity or [OH] mediate the dynamics. Based on the data shown in Table 3, it is not possible to determine whether the observed solvent-

https://doi.org/10.1021/acs.jpcb.1c06474
J. Phys. Chem. B XXXX, XXX, XXX−XXX

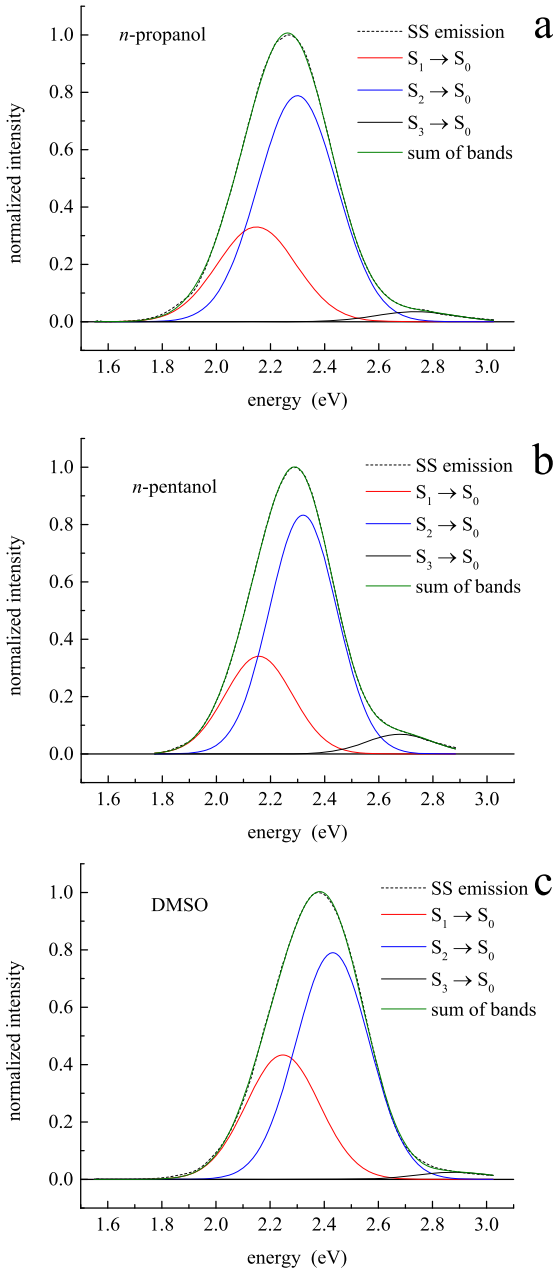

Figure 6. Steady-state fluorescence emission spectra of **FR0** in (a) *n*-propanol (PrOH), (b) *n*-pentanol (PeOH), and (c) DMSO in the frequency domain fit to three Gaussian bands. In each spectrum, the identity of each band is as indicated: (—) ss emission (unresolved), (red —) $S_1 \rightarrow S_0$ emission, (green —) $S_2 \rightarrow S_0$ emission, and (blue —) $S_3 \rightarrow S_0$ emission.

Table 3. Fitted Rate Constants for FR0 in *n*-Propanol and *n*-Pentanol

	solvent	
rate constant (Hz)	*n*-propanol ($\times 10^9$)	*n*-pentanol ($\times 10^9$)
k_{32}	9.47 ± 1.02	9.02 ± 0.22
k_{31}	1.89 ± 1.10	1.70 ± 0.20
k_{30}	1.86 ± 0.63	4.21 ± 0.50
k_{21}	2.73 ± 0.62	0.40 ± 0.15
k_{20}	3.33 ± 0.81	0.23 ± 0.14
k_{10}	0.42 ± 0.05	0.84 ± 0.26

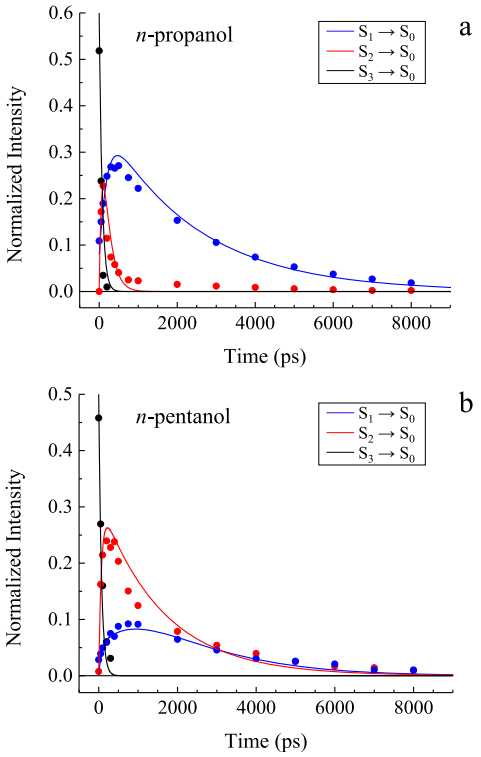

Figure 7. Normalized intensities of the three fitted bands (spectral features) extracted from the normalized time-domain data as a function of time for **FR0** in (a) *n*-propanol and (b) *n*-pentanol. The spectral features are as indicated: (—) $S_3 \rightarrow S_0$, (red —) $S_2 \rightarrow S_0$, and (blue —) $S_1 \rightarrow S_0$.

dependent changes in rate constants are dependent primarily on the hydroxyl concentration or the viscosity of the solvent. An alternative way to phrase this uncertainty is whether or not large amplitude molecular motion, such as the rotation of the diethylamino moiety, mediates the observed spectral relaxation dynamics. We can resolve this issue experimentally.

We performed a series of measurements in binary solvent systems of DMSO and *n*-propanol in which the amount of each solvent is controlled (Figure 8). The reason for the choice of DMSO and *n*-propanol as the two solvents is twofold: first, the spectral dynamics seen in *n*-propanol are not seen in DMSO and second, the two solvents have essentially the same bulk viscosity (η_{DMSO} = 1.99 cP and $\eta_{n\text{-propanol}}$ = 1.94 cP).[S6,S7] Thus, the binary solvent systems used will allow control over the hydroxyl group concentration ([OH]) under constant viscosity conditions. The data in Figure 8 show the decreasing extent of resolvable spectral dynamics with decreasing [OH]. We report the fitted rate constants for 100, 75, 50, and 25% *n*-propanol in Table 4. These data are shown graphically in Figure 9, and they reveal several interesting features. Specifically, the rate constants k_{32} and k_{31} decrease with increasing [OH], k_{20} increases with [OH] and the rate constants k_{30}, k_{21}, and k_{10} are independent of [OH]. One conclusion from these data is that the spectral dynamics we observe are associated with [OH] and not large amplitude molecular motion. This finding is consistent with the computational results (Figure 3) showing no significant accumulation of the positive charge on the amino nitrogen in any of the excited electronic states when compared to the ground state, precluding any contribution from charge-separated species.

https://doi.org/10.1021/acs.jpcb.1c06474
J. Phys. Chem. B XXXX, XXX, XXX−XXX

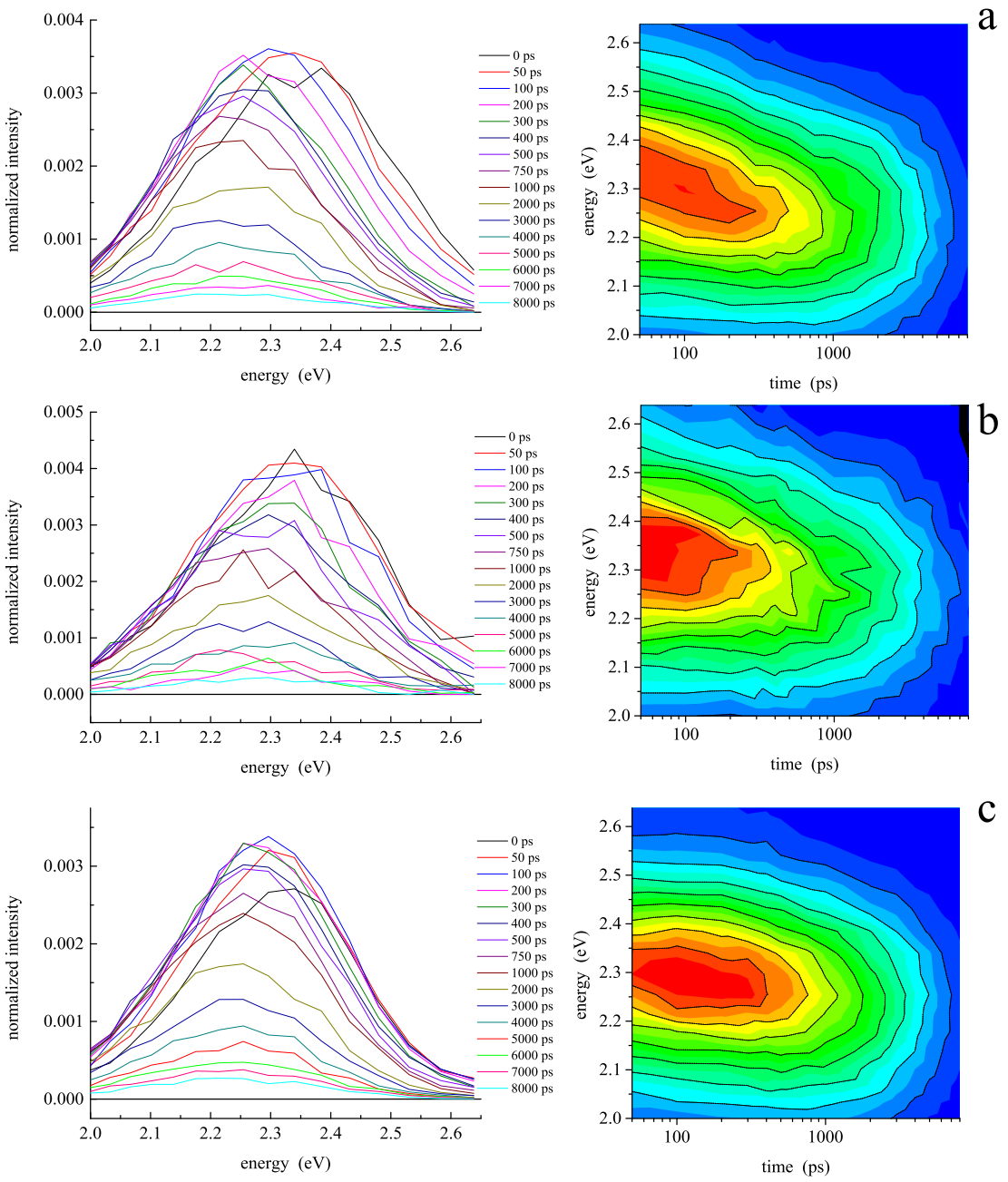

Figure 8. Time-resolved emission spectra of **FR0** in the binary solvent systems consisting of (a) 75% *n*-propanol/25% DMSO, (b) 50% *n*-propanol/50% DMSO, and (c) 25% *n*-propanol/75% DMSO extracted from the experimental fluorescence lifetime data. For the spectra in the left panels, the time corresponding to each spectrum are provided in the legends. The right panels are contour plots of the time-resolved spectra.

Table 4. Fitted Rate Constants for FR0 in *n*-Propanol/DMSO Binary Solvent Systems

	solvent			
rate constant (Hz)	*n*-propanol ($\times 10^9$)	75% *n*-propanol ($\times 10^9$)	50% *n*-propanol ($\times 10^9$)	25% *n*-propanol ($\times 10^9$)
k_{32}	9.47 ± 1.02	13.67 ± 0.26	14.64 ± 0.79	16.74 ± 1.04
k_{31}	1.89 ± 1.10	4.10 ± 0.56	4.91 ± 0.36	5.31 ± 0.50
k_{30}	1.86 ± 0.63	1.01 ± 0.34	1.76 ± 1.10	0.30 ± 0.36
k_{21}	2.73 ± 0.62	2.80 ± 0.14	2.70 ± 0.16	2.60 ± 0.60
k_{20}	3.33 ± 0.81	1.29 ± 0.13	0.80 ± 0.06	0.14 ± 0.13
k_{10}	0.42 ± 0.05	0.36 ± 0.02	0.37 ± 0.01	0.32 ± 0.04

The [OH] dependence of k_{32} and k_{31} indicates that the formation of a hydrogen bond between **FR0** and the solvent alcohol mediates the intramolecular relaxation from S_3 to both S_2 and S_1. The formation of a hydrogen bond between **FR0** and an alcohol does not, however, influence k_{30} or k_{10}. It is possible that the formation of a hydrogen bond between the

https://doi.org/10.1021/acs.jpcb.1c06474
J. Phys. Chem. B XXXX, XXX, XXX−XXX

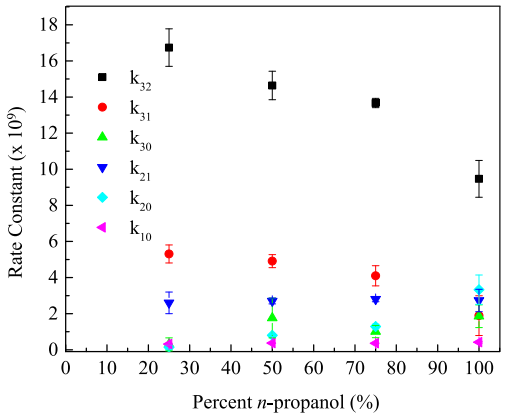

Figure 9. Fitted rate constants for **FR0** in the *n*-propanol/DMSO binary mixture as a function of percent *n*-propanol present.

alcohol proton and the **FR0** carbonyl oxygen serves to reduce the dipole moment of the excited **FR0**, thereby diminishing the dipolar coupling between the excited **FR0** and DMSO. This explanation is based on the observation that k_{3x} ($x = 0-2$) is faster than what we can measure with our instrumentation in DMSO, implying either facile quenching of S_3 by DMSO or dipolar enhancement of internal conversion in **FR0**. Similar to our previous observations in the computational studies of **FR0**-SB in its S_0 and S_1 states hydrogen bonded to alcohol solvent molecules,[6] the formation of the hydrogen bond between the alcohol proton and **FR0** carbonyl oxygen in S_2 increases the magnitude of the dipole moment relative to the gas phase value, enhancing dipolar interactions between DMSO and **FR0** in the S_2 state. An implication of these explanations for our experimental observations is that there may be observable state-dependent solvent interactions with the **FR0** chromophore.

We can test this hypothesis by examining the rotational diffusion behavior of **FR0** in *n*-propanol, *n*-pentanol, and DMSO as a function of emission wavelength, which we show in Table 5. The zero-time fluorescence anisotropy and the orientational relaxation time data in Table 5 demonstrate state-dependent reorientation dynamics for **FR0** in protic solvents and state-independent reorientation dynamics in DMSO. The reorientation time constants for **FR0** in *n*-propanol and *n*-pentanol exhibit three distinct, wavelength-dependent values, with the reorientation time being fastest in S_3 and slowest in S_2, with an S_1 reorientation being intermediate in value. There is no state dependence for **FR0** in DMSO outside the experimental uncertainty, consistent with the rapid relaxation of the higher excited singlet states in this dipolar solvent. State-dependent reorientation times have been observed previously for oxazine dyes in alcohols, where the state dependence was found to be due to the strong association between the alcohol solvent hydroxyl group and the non-bonding lone pair on the heterocyclic nitrogen.[58−61] While **FR0** does not contain an analogous nitrogen, it does manifest state-dependent changes in the electron density distributions that are central to solvent−solute interactions. While it may be tempting to speculate on the state-dependent changes in solvent interactions with **FR0** based on the measured time constants, there are several factors (e.g., local heating, hydrogen bond lifetime in each state, and competing solvent−solvent interactions) that we cannot determine with sufficient certainty. Regardless, the changes in zero-time anisotropies (seen most clearly for *n*-pentanol, determined by the angle between the excited and emitting TDM) and reorientation times (related to the volume of the reorienting entity) at different emission wavelengths demonstrate that the solvent−solute interactions of **FR0** vary in a manner that is consistent with the results of our quantum chemical computations, that is, **FR0** exhibits state-dependent rotational diffusion dynamics. For this to be the case, the lifetimes of the excited states involved must be on the order of hundreds of ps or more, consistent with the fitted results for k_{30}, k_{20}, and k_{10}.

The spectral dynamics data, taken in conjunction with the wavelength-dependent reorientation data, support our interpretation of the spectral dynamics data in the context of multiple emissive states relaxing at different rates rather than as a single electronic state exhibiting a spectral shift. The computational results indicate that the S_2 state is characterized by an electron density distribution that differs significantly from the electron density distributions seen in S_1 and S_3 (see Figures 3 and 4). The singlet state S_2 is characterized by a permanent dipole moment that is substantially smaller in magnitude than those for S_1 and S_3 (Figure 3) because the change in total electronic density associated with the $S_0 \rightarrow S_2$ transition is localized significantly on the aldehyde carbonyl functionality (Figure 4). The rate constant data and its dependence on the concentration of [OH] in solution points to the importance of dipole−dipole interactions in determining the coupling between the excited singlet states in **FR0**. Although the calculated results do not take solvent H-bonding into account, the data are consistent with the hydrogen-bonding interactions between the solvent alcohol proton and the **FR0** carbonyl oxygen modulating the dipole moment in each excited state and thereby controlling the efficiency of solvent−solute dipole−dipole interactions. It is these inter-

Table 5. Fluorescence Anisotropy and Lifetime Components for FR0 in *n*-Propanol (PrOH), *n*-Pentanol (PeOH), and DMSO[a]

λ (nm)	$R(0)$PrOH	τ_{OR} PrOH (ps)	$R(0)$PeOH	τ_{OR} PeOH (ps)	$R(0)$DMSO	τ_{OR} DMSO (ps)
490	0.17 ± 0.05	271 ± 90	0.10 ± 0.03	491 ± 98	0.17 ± 0.02	242 ± 36
500	0.19 ± 0.02	400 ± 58	0.11 ± 0.01	788 ± 53	0.19 ± 0.01	331 ± 27
520	0.17 ± 0.01	610 ± 48	0.15 ± 0.01	941 ± 45	0.18 ± 0.01	309 ± 22
540	0.17 ± 0.01	571 ± 36	0.15 ± 0.01	1250 ± 43	0.19 ± 0.01	277 ± 19
560	0.18 ± 0.01	678 ± 40	0.19 ± 0.01	1489 ± 36	0.22 ± 0.01	319 ± 24
570	0.17 ± 0.01	734 ± 32	0.21 ± 0.01	1235 ± 29	0.21 ± 0.01	351 ± 28
580	0.19 ± 0.01	512 ± 19	0.21 ± 0.01	1057 ± 30	0.26 ± 0.03	319 ± 33
590	0.22 ± 0.01	518 ± 20	0.27 ± 0.01	1057 ± 29	0.36 ± 0.04	252 ± 26

[a] $R(0)$ is the zero-time anisotropy and τ_{OR} is the orientational relaxation time constant.

https://doi.org/10.1021/acs.jpcb.1c06474
J. Phys. Chem. B XXXX, XXX, XXX−XXX

actions that appear to facilitate the relaxation between the excited singlet states.

CONCLUSIONS

We have examined the excited state relaxation dynamics of the substituted fluorene derivative **FR0**. The experimental data in conjunction with the quantum chemical calculations reveal that relaxation between three excited singlet electronic states accounts for the spectral relaxation dynamics observed for **FR0** in protic solvents. The relaxation dynamics are related to the concentration of hydroxyl functionality in the solvent system, indicating that hydrogen bonding between the aldehyde oxygen of **FR0** in the S_2 state and the solvent hydroxyl proton diminishes the role of dipolar solvent−solute coupling, reducing the relaxation rates for some of the relaxation pathways. Further experimentation will be required to address in detail the dependence of the electronic state coupling and its dependence on solvent interactions on chemical structures.

AUTHOR INFORMATION

Corresponding Author

G. J. Blanchard − *Department of Chemistry, Michigan State University, East Lansing, Michigan 48824, United States;* orcid.org/0000-0002-1207-0810; Phone: +1 517 353 1105; Email: blanchard@chemistry.msu.edu

Authors

Briana A. Capistran − *Department of Chemistry, Michigan State University, East Lansing, Michigan 48824, United States*

Stephen H. Yuwono − *Department of Chemistry, Michigan State University, East Lansing, Michigan 48824, United States;* orcid.org/0000-0002-6604-3543

Mehdi Moemeni − *Department of Chemistry, Michigan State University, East Lansing, Michigan 48824, United States*

Soham Maity − *Department of Chemistry, Michigan State University, East Lansing, Michigan 48824, United States*

Aria Vahdani − *Department of Chemistry, Michigan State University, East Lansing, Michigan 48824, United States*

Babak Borhan − *Department of Chemistry, Michigan State University, East Lansing, Michigan 48824, United States;* orcid.org/0000-0002-3193-0732

James E. Jackson − *Department of Chemistry, Michigan State University, East Lansing, Michigan 48824, United States;* orcid.org/0000-0002-4506-7415

Piotr Piecuch − *Department of Chemistry, Michigan State University, East Lansing, Michigan 48824, United States; Department of Physics and Astronomy, Michigan State University, East Lansing, Michigan 48824, United States;* orcid.org/0000-0002-7207-1815

Marcos Dantus − *Department of Chemistry, Michigan State University, East Lansing, Michigan 48824, United States; Department of Physics and Astronomy, Michigan State University, East Lansing, Michigan 48824, United States;* orcid.org/0000-0003-4151-5441

Complete contact information is available at: https://pubs.acs.org/10.1021/acs.jpcb.1c06474

Notes

The authors declare no competing financial interest.

ACKNOWLEDGMENTS

The collaboration between synthesis, theory, and experiments for the understanding and development of super photoreagents for precision chemistry is funded by a seed grant from DARPA and AMRDEC (W31P4Q-20-1-0001). Partial support comes from NIH (grant nos. 2R01EY016077-08A1 and 5R01EY025383-02 R01 to G.J.B., and R01GM101353 to B.B.), NSF (grant no. CHE1836498 to M.D.), and the U.S. DOE (grant no. DE-FG02-01ER15228 to P.P.). This work was supported in part through computational resources and services provided by the Institute for Cyber-Enabled Research at Michigan State University. The views and conclusions contained in this document are those of the authors and should not be interpreted as representing the official policies, either expressed or implied, of the Defense Advanced Research Projects Agency, the U.S. Army, or the U.S. Government. The authors would like to thank Dr. Ilias Magoulas for providing the code used in generating the electronic density difference maps shown in this work.

REFERENCES

(1) Malval, J.-P.; Diemer, V.; Savary, F. M.; Jacques, P.; Allonas, X.; Chaumeil, H.; Defoin, A.; Carré, C. Excited state proton transfer in a 'super' photoacid based on a phenol-pyridinium biaryl chromophore. *Chem. Phys. Lett.* **2008**, *455*, 238−241.

(2) Finkler, B.; Spies, C.; Vester, M.; Walte, F.; Omlor, K.; Riemann, I.; Zimmer, M.; Stracke, F.; Gerhards, M.; Jung, G. Highly photostable ″super″-photoacids for ultrasensitive fluorescence spectroscopy. *Photochem. Photobiol. Sci.* **2014**, *13*, 548−562.

(3) Hunt, J. R.; Dawlaty, J. M. Photodriven Deprotonation of Alcohols by a Quinoline Photobase. *J. Phys. Chem. A* **2018**, *122*, 7931−7940.

(4) Hunt, J. R.; Dawlaty, J. M. Kinetic Evidence for the Necessity of Two Proton Donor Molecules for Successful Excited State Proton Transfer by a Photobase. *J. Phys. Chem. A* **2019**, *123*, 10372−10380.

(5) Lahiri, J.; Moemeni, M.; Kline, J.; Borhan, B.; Magoulas, I.; Yuwono, S. H.; Piecuch, P.; Jackson, J. E.; Dantus, M.; Blanchard, G. J. Proton Abstraction Mediates Interactions between the Super Photobase FR0-SB and Surrounding Alcohol Solvent. *J. Phys. Chem. B* **2019**, *123*, 8448−8456.

(6) Lahiri, J.; Moemeni, M.; Kline, J.; Magoulas, I.; Yuwono, S. H.; Laboe, M.; Shen, J.; Borhan, B.; Piecuch, P.; Jackson, J. E.; et al. Isoenergetic Two-Photon Excitation Enhances Solvent-to-Solute Excited-State Proton Transfer. *J. Chem. Phys.* **2020**, *153*, 224301.

(7) Lahiri, J.; Moemeni, M.; Magoulas, I.; Yuwono, S. H.; Kline, J.; Borhan, B.; Piecuch, P.; Jackson, J. E.; Blanchard, G. J.; Dantus, M. Steric Effects in Light-Induced Solvent Proton Abstraction. *Phys. Chem. Chem. Phys.* **2020**, *22*, 19613−19622.

(8) Sheng, W.; Nairat, M.; Pawlaczyk, P. D.; Mroczka, E.; Farris, B.; Pines, E.; Geiger, J. H.; Borhan, B.; Dantus, M. Ultrafast Dynamics of a "Super" Photobase. *Angew. Chem., Int. Ed.* **2018**, *57*, 14742−14746.

(9) Kucherak, O. A.; Didier, P.; Mély, Y.; Klymchenko, A. S. Fluorene Analogues of Prodan with Superior Fluorescence Brightness and Solvatochromism. *J. Phys. Chem. Lett.* **2010**, *1*, 616−620.

(10) Pillman, H. A.; Blanchard, G. J. Effects of Energy Dissipation on Motional Dynamics in Unilamellar Vesicles. *J. Phys. Chem. B* **2010**, *114*, 13703−13709.

(11) Baumler, S. M. Diffusional Motion as a Gauge of Interfacial Fluidity and Adhesion of Supported Model Membrane Films. Ph.D. Dissertation, Michigan State University, East Lansing, MI, 2017.

(12) Kohn, W.; Sham, L. J. Self-Consistent Equations including Exchange and Correlation Effects. *Phys. Rev.* **1965**, *140*, A1133−A1138.

(13) Hohenberg, P.; Kohn, W. Inhomogeneous Electron Gas. *Phys. Rev.* **1964**, *136*, B864−B871.

(14) Yanai, T.; Tew, D. P.; Handy, N. C. A new hybrid exchange-correlation functional using the Coulomb-attenuating method (CAM-B3LYP). *Chem. Phys. Lett.* **2004**, *393*, 51−57.
(15) Hehre, W. J.; Ditchfield, R.; Pople, J. A. Self-Consistent Molecular Orbital Methods. XII. Further Extensions of Gaussian-type Basis Sets for Use in Molecular Orbital Studies of Organic Molecules. *J. Chem. Phys.* **1972**, *56*, 2257−2261.
(16) Hariharan, P. C.; Pople, J. A. The Influence of Polarization Functions on Molecular Orbital Hydrogenation Energies. *Theor. Chim. Acta* **1973**, *28*, 213−222.
(17) Clark, T.; Chandrasekhar, J.; Spitznagel, G. W.; Schleyer, P. V. R. Efficient diffuse function-augmented basis sets for anion calculations. III. The 3-21+G basis set for first-row elements, Li-F. *J. Comp. Chem.* **1983**, *4*, 294−301.
(18) Stanton, J. F.; Bartlett, R. J. The equation of motion coupled-cluster method. A systematic biorthogonal approach to molecular excitation energies, transition probabilities, and excited state properties. *J. Chem. Phys.* **1993**, *98*, 7029−7039.
(19) Čížek, J. On the Correlation Problem in Atomic and Molecular Systems. Calculation of Wavefunction Components in Ursell-Type Expansion using Quantum-Field Theoretical Methods. *J. Chem. Phys.* **1966**, *45*, 4256−4266.
(20) Purvis, G. D., III; Bartlett, R. J. A full coupled-cluster singles and doubles model: The inclusion of disconnected triples. *J. Chem. Phys.* **1982**, *76*, 1910−1918.
(21) Fradelos, G.; Lutz, J. J.; Wesołowski, T. A.; Piecuch, P.; Włoch, M. Embedding vs Supermolecular Strategies in Evaluating the Hydrogen-Bonding-Induced Shifts of Excitation Energies. *J. Chem. Theory Comput.* **2011**, *7*, 1647−1666.
(22) Piecuch, P.; Gour, J. R.; Włoch, M. Left-Eigenstate Completely Renormalized Equation-of-Motion Coupled-Cluster Methods: Review of Key Concepts, Extension to Excited States of Open-Shell Systems, and Comparison with Electron-Attached and Ionized Approaches. *Int. J. Quantum Chem.* **2009**, *109*, 3268−3304.
(23) Włoch, M.; Lodriguito, M. D.; Piecuch, P.; Gour, J. R. Two New Classes of Non-Iterative Coupled-Cluster Methods Derived from the Method of Moments of Coupled-Cluster Equations. *Mol. Phys.* **2006**, *104*, 2149−2172. Erratum, *Mol. Phys.* **2006**, *104*, 2991.
(24) Barca, G. M. J.; Bertoni, C.; Carrington, L.; Datta, D.; De Silva, N.; Deustua, J. E.; Fedorov, D. G.; Gour, J. R.; Gunina, A. O.; Guidez, E.; et al. Recent Developments in the General Atomic and Molecular Electronic Structure System. *J. Chem. Phys.* **2020**, *152*, 154102.
(25) Gordon, M. S.; Schmidt, M. W. Advances in Electronic Structure Theory: GAMESS a Decade Later. In *Theory and Applications of Computational Chemistry: The First Forty Years*; Dykstra, C. E., Frenking, G., Kim, K. S., Scuseria, G. E., Eds.; Elsevier: Amsterdam, 2005, pp 1167−1189.
(26) Kowalski, K.; Piecuch, P. New Coupled-Cluster Methods with Singles, Doubles, and Noniterative Triples for High Accuracy Calculations of Excited Electronic States. *J. Chem. Phys.* **2004**, *120*, 1715−1738.
(27) Piecuch, P.; Kucharski, S. A.; Kowalski, K.; Musiał, M. Efficient Computer Implementation of the Renormalized Coupled-Cluster Methods: The R-CCSD[T], R-CCSD(T), CR-CCSD[T], and CR-CCSD(T) Approaches. *Comput. Phys. Commun.* **2002**, *149*, 71−96.
(28) Włoch, M.; Gour, J. R.; Kowalski, K.; Piecuch, P. Extension of Renormalized Coupled-Cluster Methods Including Triple Excitations to Excited Electronic States of Open-Shell Molecules. *J. Chem. Phys.* **2005**, *122*, 214107.
(29) Humphrey, W.; Dalke, A.; Schulten, K. VMD: Visual Molecular Dynamics. *J. Mol. Graphics* **1996**, *14*, 33−38.
(30) Maroncelli, M.; Fleming, G. R. Picosecond Solvation Dynamics of Coumarin 153: The Importance of Molecular Aspects of Solvation. *J. Chem. Phys.* **1987**, *86*, 6221−6239.
(31) Maroncelli, M.; Fleming, G. R. Comparison of Time-Resolved Fluorescence Stokes Shift Measurements to a Molecular Theory of Solvation Dynamics. *J. Chem. Phys.* **1988**, *89*, 875−881.
(32) Nagarajan, V.; Brearley, A. M.; Kang, T. J.; Barbara, P. F. Time-Resolved Spectroscopic Measurements on Microscopic Solvation Dynamics. *J. Chem. Phys.* **1987**, *86*, 3183−3196.
(33) Simon, J. D.; Su, S.-G. Picosecond Stokes Shift Studies of Solvent Friction: Experimental Measurements of Time-Dependent Band Shape and Integrated Intensity. *Chem. Phys.* **1991**, *152*, 143−152.
(34) Su, S. G.; Simon, J. D. Solvation Dynamics in Ethanol. *J. Phys. Chem.* **1987**, *91*, 2693−2696.
(35) Bagchi, B.; Oxtoby, D. W.; Fleming, G. R. Theory of the Time Development of the Stokes Shift in Polar Media. *Chem. Phys.* **1984**, *86*, 257−267.
(36) Castner, E. W., Jr.; Fleming, G. R.; Bagchi, B. Influence of Non-Debye Relaxation and of Molecular Shape on the Time Dependence of the Stokes Shift in Polar Media. *Chem. Phys. Lett.* **1988**, *143*, 270−276.
(37) Castner, E. W., Jr.; Maroncelli, M.; Fleming, G. R. Subpicosecond Resolution Studies of Solvation Dynamics in Polar Aprotic and Alcohol Solvents. *J. Chem. Phys.* **1987**, *86*, 1090−1097.
(38) Eom, I.; Joo, T. Polar Solvation Dynamics of Coumarin 153 by Ultrafast Time-Resolved Fluorescence. *J. Chem. Phys.* **2009**, *131*, 244507.
(39) Böhmer, R.; Gainaru, C.; Richert, R. Structure and dynamics of monohydroxy alcohols-Milestones towards their microscopic understanding, 100 years after Debye. *Phys. Rep.* **2014**, *545*, 125−195.
(40) Adhikary, R.; Barnes, C. A.; Petrich, J. W. Solvation Dynamics of the Fluorescent Probe PRODAN in Heterogeneous Environments: Contributions from the Locally Excited and Charge-Transferred States. *J. Phys. Chem. B* **2009**, *113*, 11999−12004.
(41) Middelhoek, E. R.; van der Meulen, P.; Verhoeven, J. W.; Glasbeek, M. Picosecond Time-Dependent Stokes Shift Studies of Fluoroprobe in Liquid Solution. *Chem. Phys.* **1995**, *198*, 373−380.
(42) Middelhoek, E. R.; Zhang, H.; Verhoeven, J. W.; Glasbeek, M. Subpicosecond Studies of the Solvation Dynamics of Fluoroprobe in Liquid Solution. *Chem. Phys.* **1996**, *211*, 489−497.
(43) Hermant, R. M.; Bakker, N. A. C.; Scherer, T.; Krijnen, B.; Verhoeven, J. W. Systematic study of a Series of Highly Fluorescent Rod-Shaped Donor-Acceptor Systems. *J. Am. Chem. Soc.* **1990**, *112*, 1214−1221.
(44) Silori, Y.; Dey, S.; De, A. K. How to Study Picosecond Solvation Dynamics Using Fluorescent Probes with Small Stokes Shifts. *Chem. Phys. Lett.* **2018**, *693*, 222−226.
(45) Hébert, P.; Baldacchino, G.; Gustavsson, T.; Mialocq, J.-C. Sub-Picosecond Fluorescence Study of the LDS 751 Dye Molecule in Ethanol. *Chem. Phys. Lett.* **1993**, *213*, 345−350.
(46) Blanchard, G. J. Time-resolved measurement of the stimulated emission Stokes shift in LDS750: Evidence for inhomogeneous relaxation kinetics. *J. Chem. Phys.* **1991**, *95*, 6317−6325.
(47) Agmon, N. Dynamic Stokes Shift in Coumarin: Is it Only Relaxation? *J. Phys. Chem.* **1990**, *94*, 2959−2963.
(48) McCarthy, P. K.; Blanchard, G. J. AM1 Study of the Electronic Structure of Coumarins. *J. Phys. Chem.* **1993**, *97*, 12205−12209.
(49) Jiang, Y.; McCarthy, P. K.; Blanchard, G. J. The role of multiple electronic states in the dissipative nergy dynamics of coumarin 153. *Chem. Phys.* **1994**, *183*, 249−267.
(50) Eber, G.; Grüneis, F.; Schneider, S.; Dörr, F. Dual Fluorescence Emission of Azulene Derivatives in Solution. *Chem. Phys. Lett.* **1974**, *29*, 397−404.
(51) Huppert, D.; Jortner, J.; Rentzepis, P. M. $S_2 \rightarrow S_1$ Emission of Azulene in Solution. *Chem. Phys. Lett.* **1972**, *13*, 225−228.
(52) Orlandi, G.; Siebrand, W. Mechanisms of Vibronic Intensity Borrowing. *Chem. Phys. Lett.* **1972**, *15*, 465−468.
(53) Orlandi, G.; Siebrand, W. Theory of vibronic intensity borrowing. Comparison of Herzberg-Teller and Born-Oppenheimer coupling. *J. Chem. Phys.* **1973**, *58*, 4513−4523.
(54) Karpovich, D. S.; Blanchard, G. J. Relating the Polarity-Dependent Fluorescence Response of Pyrene to Vibronic Coupling. Achieving a Fundamental Understanding of the py Polarity Scale. *J. Phys. Chem.* **1995**, *99*, 3951−3958.

https://doi.org/10.1021/acs.jpcb.1c06474
J. Phys. Chem. B XXXX, XXX, XXX−XXX

(55) Geldof, P. A.; Rettschnick, R. P. H.; Hoytink, G. J. Vibronic Coupling and Radiative Transitions. *Chem. Phys. Lett.* **1971**, *10*, 549−558.
(56) LeBel, R. G.; Goring, D. A. I. Density, Viscosity, Refractive Index, and Hygroscopicity of Mixtures of Water and Dimethyl Sulfoxide. *J. Chem. Eng. Data* **1962**, *7*, 100−101.
(57) Mikhail, S. Z.; Kimel, W. R. Densities and Viscosities of 1-Propanol-Water Mixtures. *J. Chem. Eng. Data* **1963**, *8*, 323−328.
(58) Blanchard, G. J.; Cihal, C. A. Orientational relaxation dynamics of oxazine 118 and resorufin in the butanols. Valence- and state-dependent solvation effects. *J. Phys. Chem.* **1988**, *92*, 5950−5954.
(59) Blanchard, G. J. A Study of the State-Dependent Reorientation Dynamics of Oxazine 725 in Primary Normal Aliphatic Alcohols. *J. Phys. Chem.* **1988**, *92*, 6303−6307.
(60) Blanchard, G. J. State-dependent reorientation characteristics of Methylene Blue: the importance of dipolar solvent-solute interactions. *J. Phys. Chem.* **1989**, *93*, 4315−4319.
(61) Blanchard, G. J. Detection of a transient solvent-solute complex using time-resolved pump-probe spectroscopy. *Anal. Chem.* **1989**, *61*, 2394−2398.

https://doi.org/10.1021/acs.jpcb.1c06474
J. Phys. Chem. B XXXX, XXX, XXX−XXX